Ickrath, M., Bohnhoff, M., Dresen, G., Martinez Garzon, P., Bulut, F., Kwiatek, G., Germer, O. (2015): Detailed analysis of spatiotemporal variations of the stress field orientation along the Izmit-Düzce rupture in NW Turkey from inversion of first-motion polarity data. - *Geophysical Journal International*, *202*, 3, pp. 2120—2132.

DOI: http://doi.org/10.1093/gji/ggv273

Geophysical Journal International

Geophys. J. Int. (2015) **202,** 2120–2132 doi: 10.1093/gji/ggv273
GJI Seismology

Detailed analysis of spatiotemporal variations of the stress field orientation along the Izmit-Düzce rupture in NW Turkey from inversion of first-motion polarity data

Michèle Ickrath,[1] Marco Bohnhoff,[1,2] Georg Dresen,[1] Patricia Martínez-Garzón,[1] Fatih Bulut,[1,*] Grzegorz Kwiatek[1] and Oliver Germer[1]

[1]*Helmholtz Centre Potsdam GFZ German Research Centre for Geosciences, Section 3.2: Geomechanics and Rheology, Telegrafenberg, Potsdam, Germany. E-mail: bohnhoff@gfz-potsdam.de*
[2]*Free University Berlin, Department of Earth Sciences, Malteser Strasse* 74-100, *D*-12249 *Berlin, Germany*

Accepted 2015 June 22. Received 2015 June 21; in original form 2015 February 10

SUMMARY

We investigate spatiotemporal variations of the crustal stress field orientation along the rupture zones of the 1999 August Izmit M_w 7.4 and November Düzce M_w 7.1 earthquakes at the North Anatolian Fault zone (NAFZ) in NW Turkey. Our primary focus is to elaborate on the relation between the state of the crustal stress field and distinct seismotectonic features as well as variations of coseismic slip within the seismogenic layer of the crust. To achieve this, we compile an extensive data base of hypocentres and first-motion polarities including a newly derived local hypocentre catalogue extending from 2 yr prior (1997) to 2 yr after (2001) the Izmit and Düzce main shocks. This combined data set allows studying spatial and temporal variations of stress field orientation along distinct fault segments for the pre- and post-seimic phase of the two large earthquakes in detail. Furthermore, the occurrence of two $M > 7$ earthquakes in rapid succession gives the unique opportunity to analyse the 87-d-long 'inter-seismic phase' between them. We use the MOTSI (first MOTion polarity Stress Inversion) procedure directly inverting first-motion polarities to study the stress field evolution of nine distinct segments. In particular, this allows to determine the stress tensor also for the pre- and post-seismic phases when no stable single-event focal mechanisms can be determined. We observe significantly different stress field orientations along the combined 200-km-long rupture in accordance with lateral variations of coseismic slip and seismotectonic setting. Distinct vertical linear segments of the NAFZ show either pure-strike slip behaviour or transtensional and normal faulting if located near pull-apart basins. Pull-apart structures such as the Akyazi and Düzce basins show a predominant normal faulting behaviour along the NAFZ and reflect clearly different characteristic from neighbouring strike-slip segments. Substantial lateral stress field heterogeneity following the two main shocks is observed that declines with time towards the post-seismic period that rather reflects the regional right-lateral strike-slip stress field.

Key words: Earthquake dynamics; Earthquake source observations; Seismicity and tectonics.

1 INTRODUCTION

The North Anatolian Fault Zone (NAFZ) in NW Turkey is one of the most active and best studied strike-slip faults and has produced several destructive ($M > 7$) earthquakes during the last century (Toksöz *et al.* 1979; Barka 1999; Hubert-Ferrari *et al.* 2000; Şengör *et al.* 2005; Bohnhoff *et al.* 2013). Due to its recent sequence of two subsequent $M > 7$ earthquakes in 1999 the fault zone provides an unique opportunity to study earthquake-related processes such as stress accumulation and release during the seismic cycle, earthquake rupture processes and fault segmentation in space and time (Fig. 1). Recent studies have identified substantial along-rupture and temporal variations of the local stress tensor in conjunction with the 1999 Izmit $M_W = 7.4$ earthquake (Bohnhoff *et al.* 2006; Ickrath *et al.* 2014). Those stress variations were in good agreement with the stress recovery model (Michael 1987) and also pointed

*Now at: AFAM Research Center, Istanbul Aydın University, 34295 İstanbul, Turkey.

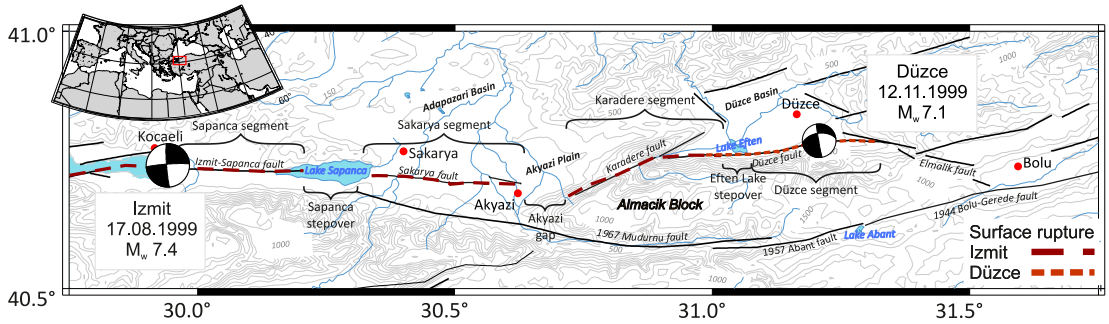

Figure 1. Segmentation along the North Anatolian Fault Zone (NAFZ) associated with the surface fault ruptures of 1999 August 17 Izmit (Sapanca segment, Sakarya segment and Karadere segment from west to east) and 1999 November 12 Düzce (Düzce segment) earthquakes (after Barka *et al.* 2002). In addition the prominent extensional step-overs are combined from Langridge *et al.* (2002) and Lettis *et al.* (2002). Faults are taken from Langridge *et al.* (2002).

out the role of local changes of the seismotectonic setting for the local crustal stress field orientation. Based on the previous studies, a substantially enlarged dataset of local seismicity was derived within this study based on recordings from the local SApanca-BOlu seismic NETwork (SABONET, Milkereit *et al.* 2000) for the time span 1997–2001, that is from 2 yr prior to 2 yr after the $M > 7$ Izmit and Düzce 1999 earthquakes. While the previous studies focused on the 2-month Izmit aftershock period based on the inversion of aftershock focal mechanisms along the Izmit rupture, the main focus here is to also include the local stress field orientation during the pre-seismic phase (years 1997/1998), the entire inter Izmit-Düzce phase, and the post-seismic phase (years 2000/2001). For the determination of the stress field orientation the direct inversion of first-motion *P*-wave polarity data has been performed using the MOTSI method (Abers & Gephart 2001). The main benefit of the direct inversion of first-motion polarity data is that even areas without stable single-event focal mechanisms can be studied using all available polarities from local seismicity clusters and inverting them for the local stress tensor. With this approach, it is possible to determine the stress field orientation for areas of the Izmit and Düzce ruptures before and after activation for which otherwise no local stress field orientation could be determined due to limitation in available data and since too few or no single-event focal mechanisms were available. Integrating recordings from Düzce aftershocks and using the MOTSI technique allows for the first time gaining insight into the stress field evolution of the easternmost segments of the Izmit and Düzce ruptures and the so far poorly studied area of the Elmalik fault representing the transition of the Düzce rupture to the 1944 *M* 7.3 rupture.

2 DATA AND METHOD

Seismic waveform recordings from the permanent SABONET were analysed to better resolve the stress field orientation and changes in the broader Izmit-Sapanca, Düzce and Bolu areas (Figs 1 and 2). SABONET consists of 15 stations equipped with Mark L4–3-D 1 Hz seismometers, 24-bit digitizers operated at a sampling rate of 100 Hz and global positioning system (GPS) timing (Milkereit *et al.* 2000; Baumbach *et al.* 2003; Bindi *et al.* 2007). SABONET was operated in event triggering mode during the time period considered here (1997–2001) except for the 2-month Izmit aftershock sequence when it was switched to continuous recording. Due to the large false triggering of events caused by the noise conditions and the great number of aftershocks (approximately 40 000 aftershocks, 2000 triggers on the day following the Izmit mainshock to still 100 triggers per day in the beginning of November (Milkereit *et al.* 2000) a refined trigger algorithm was used (a smaller STA window to separate multiple events). For the absolute hypocentre determination of local seismicity the HYPOCENTER location program (Lienert *et al.* 1986; Lienert & Havskov 1995) based on HYPO71 (Lee & Lahr 1972) was applied to manually derived phase picks using an optimized 1-D local velocity model (Bulut *et al.* 2007). In this study, a total of ∼9000 events were detected of which 4062 could be located for the time period 1997–2001.

For the inter Izmit-Düzce phase (1999 August–November) also data from the temporary German Task Force for earthquakes (GTF) network deployed by the Helmholtz-Centre Potsdam GFZ were used (Zschau, personal communication). The GTF network consisted of 21 short-period stations and was in operation for a period of 60 d between 4 d after the Izmit earthquake until 1999 October 21 (Grosser *et al.* 1998; Baumbach *et al.* 2003). The GTF network was deployed by invitation from the General Directorate of Disasters Affairs in Ankara and stations were distributed mainly west of Adapazari to monitor the aftershock activity in the Izmit epicentral region and to increase the coverage of the SABONET (Milkereit *et al.* 2000; Parolai *et al.* 2004; Figs 1 and 2) towards a reduced average station spacing of 15 km. Waveforms were sampled at 100 samples per second and the aftershock event catalogue consisted of >10 000 earthquakes of which 4700 were relocated using the double-difference technique reaching a relative precision of about 300 m (Bulut *et al.* 2007). For this study and for the first time we also included newly determined aftershock seismicity from the Akyazi-Karadere (eastern Izmit rupture) and Düzce-Elmalik segments (692 events, see grey dots in Fig. 2 inter Izmit-Düzce phase) for which *P*-wave polarities were picked in addition to the already processed *P*- and *S*-wave arrival times. Fig. 3 summarizes the location errors and number of *P*- and *S*-picks for the data set considered here. The combined high-quality data set consisting of SABONET recordings (1997–2001) and the 2-month combined GTF-SABONET data is well suited to investigate potential local temporal and spatial variations of the stress field and to include the previously less-well covered areas where not enough single-event focal mechanisms were available to invert for the stress field (Ickrath *et al.* 2014). Fig. 2 illustrates the seismicity catalogue used for this study separated in the pre-seismic, inter Izmit-Düzce and post-seismic phase in relation to the Izmit and Düzce epicentres.

For the calculation of the stress field orientation, a direct inversion of earthquake first-motion polarities was performed using the MOTSI (first MOTion Stress Inversion) procedure of Abers & Gephart (2001). MOTSI follows a non-linear inversion scheme, which is built on the Focal Mechanism Stress Inversion (FMSI)

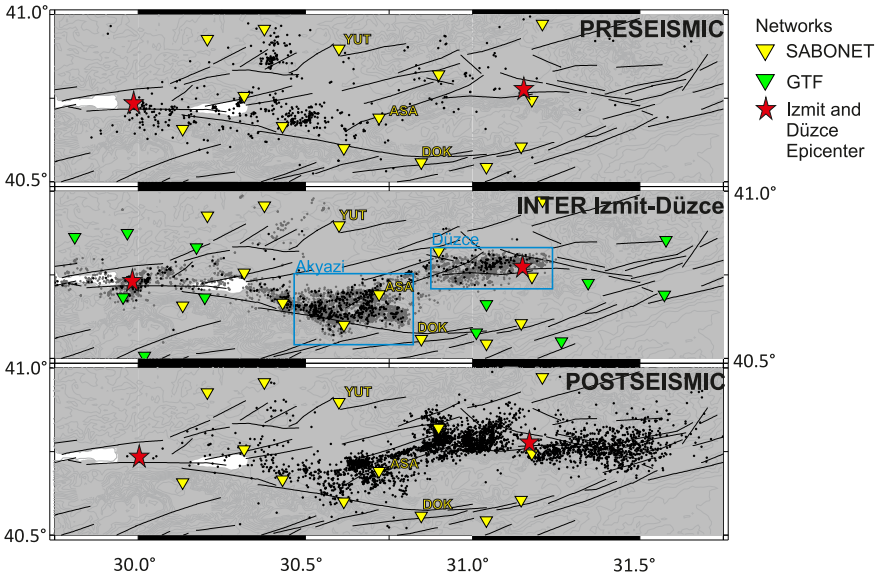

Figure 2. Earthquake epicentre database throughout the study area for the pre-seismic, inter Izmit-Düzce and post-seismic phase derived from of the GTF and SABONET networks used for the stress tensor inversion based on first-motion polarities. Black dots represent the epicentre catalogue of the 4062 newly located and processed events from the SABONET (this study). Grey dots indicate the 692 selected events from the joint GTF/SABONET network that were used for a better resolution for the inter Izmit-Düzce phase in the Akyazi and Düzce area (Bulut *et al.* 2007) (blue boxes).

algorithm of Gephart (1990) computing the stress tensor from first-motion polarities rather than from focal mechanisms. Additional to the Wallace–Bott criteria it is assumed that all motions on a fault within a specific volume of the crust are due to the same orientation of the stress tensor (homogeneity of the stress field in the studied area). The inversion uses two-nested grid-searches to estimate the best possible fit for stress parameters and the focal mechanism consistent with both the calculated stress and the first motions. The outer search is sequentially testing independent stress models. The inner search is calculating a suite of stress consistent focal mechanisms for each stress model over a grid of fault planes for each event. In the last step, each stress consistent focal mechanism will be compared to the first motions to find the best fitting solution. Then, the confidence intervals are estimated by numerically integrating the marginal probability density functions of the fittings of the first-motion polarities in the focal mechanisms.

The main advantage of this method is that through using directly first-motion polarities additional uncertainties during the determination of focal mechanisms can be avoided since every focal mechanism as input for the stress inversion has an uncertainty of typically not less than 10° (e.g. Bohnhoff *et al.* 2004). Another reason for using this method is that the small number of only 15 stations (SABONET) rarely allowed the determination of stable single-event focal mechanism due to the limited coverage of stations on the focal sphere. And finally, especially the numerous smaller events where focal mechanism determination is limited are of special interest to increase the database. The advantage of MOTSI is that the entire set of polarity observations are considered, although they would not lead to single-event focal mechanisms. The basic assumption behind this is that smaller earthquakes $M \leq 3$ preferentially occur on faults with orientation clustered along the larger pre-existing main fault with the maximum Coulomb failure stress (Robinson & McGinty 2000). The regional stress tensors vary in space, but Robinson & McGinty (2000) confirmed that with a large number of events the average stress tensor can still be well resolved with the direct inversion of first motion polarities.

Although Abers & Gephart (2001) suggest to use more than 20 first-motion polarities per event here the idea from Robinson & McGinty (2000) is applied which uses the approach for direct inversion of first motion polarity especially for spare networks with a number of first motion polarities smaller than 13 per event. If those events are clustered in space and time, a local homogeneous stress field in the hypocentre area can be assumed (in our case nine spatial clusters as introduced in the following section). They also compared and confirmed the results to the inversion from focal mechanism data. To confirm results, the inter Izmit-Düzce phase is compared to the results from the previous study obtained from focal mechanism inputs.

3 SEISMICITY CLUSTERS

Studying a region for potential spatial and/or temporal stress field variations requires a careful division of the target region into subareas (spatial bins) and separate inversion for the stress tensor orientation in each subarea. Hardebeck & Hauksson (2000) and Townend & Zoback (2000) discussed the different binning of subareas and the influence on the obtained stress field orientation with regard to the potential to resolve stress changes along the San Andreas Fault (SAF) and with distance to the main fault branch. Whereas Hardebeck & Hauksson (2000) used bins perpendicular to the fault, Townend & Zoback (2000) used a subset derived from the recursive gridding method, which resulted in bins corresponding to the density of data in an area and with a higher weighting in seismically active areas fulfilling the basic assumption of stress homogeneity. Hardebeck & Hauksson (2000) and Townend & Zoback (2000) found different stress orientations near the San Andreas fault which was initially attributed to different binning schemes used in these studies. However, Hardebeck & Michael (2004) showed that the different stress orientations are mainly due to extrapolation of stress orientations to regions without or with insufficient data. Taking this into consideration, the hypocentre catalogue along the Izmit and

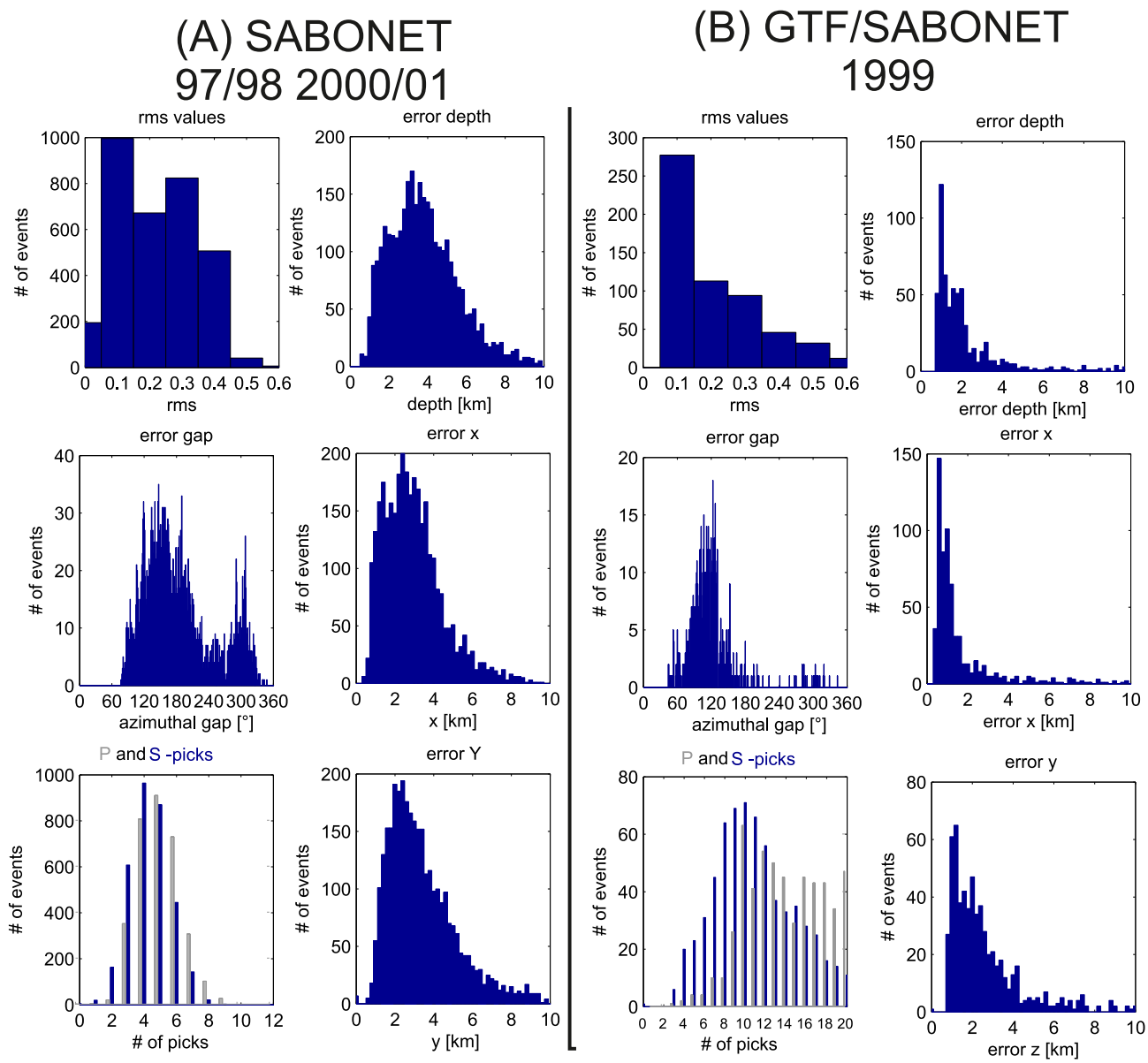

Figure 3. (a) Rms values, vertical and horizontal location errors, azimuthal gap, and number of *P* and *S* picks per event for the obtained hypocentre catalogue of 4062 events recorded by the SABONET network (see text for details). (b) Same as in (a) but for the inter Izmit-Düzce phase using 692 selected events from the relocated earthquake hypocentre catalogue from Bulut *et al.* (2007) (see text for details).

Düzce ruptures is analysed for stationary spatial seismicity clusters for each of the considered time periods to resolve the stress field and its potential perturbations on a local scale. The results are related to the segmentation of the NAFZ, and used to detect and investigate potential temporal variations of the local stress tensor (Bohnhoff *et al.* 2006; Ickrath *et al.* 2014). Our approach differs from the methods used by Townend & Zoback (2000) and Hardebeck & Hauksson (2000) in using first-motion polarities rather than focal mechanism for the stress inversion and the number of seismic events (SAF $\sim$ 50 000 events). Here the seismicity clusters are analysed based on the polarity distribution and event locations. To avoid potential binning effects only events from areas that are large enough and time intervals with enough events ($>$15) are inverted to allow for a stable determination of the local stress tensor. In our analysis scheme, the first step is to test the quality of the picked first-motion polarities by separately plotting positive and negative first-motion polarities for each station of the seismic network for different spatial seismicity clusters (for details see Bulut *et al.* 2012, their fig. 9; Fig. 4). Besides a general quality test another idea behind this was to see whether the particular clusters can be represented by a single faulting mechanism

Fig. 4 gives two examples for stations ASA and DOK (see Fig. 2 for station locations). In addition, the *S*–*P* times are plotted to show spatial proximity of selected events. Results show that the picked first-motion polarities are consistent and of good quality. In addition, we also plot the first-motion polarities of located events for each station for different time periods separately. Examples for station DOK and YUT for the pre-seismic year 1997 and post-seismic year 2000 are shown in Fig. 5, respectively. The positive and negative first-motion polarities marked by the green crosses and red circles, respectively, lead to a first recognition of areas with possible different faulting mechanisms. Combined with the analysis

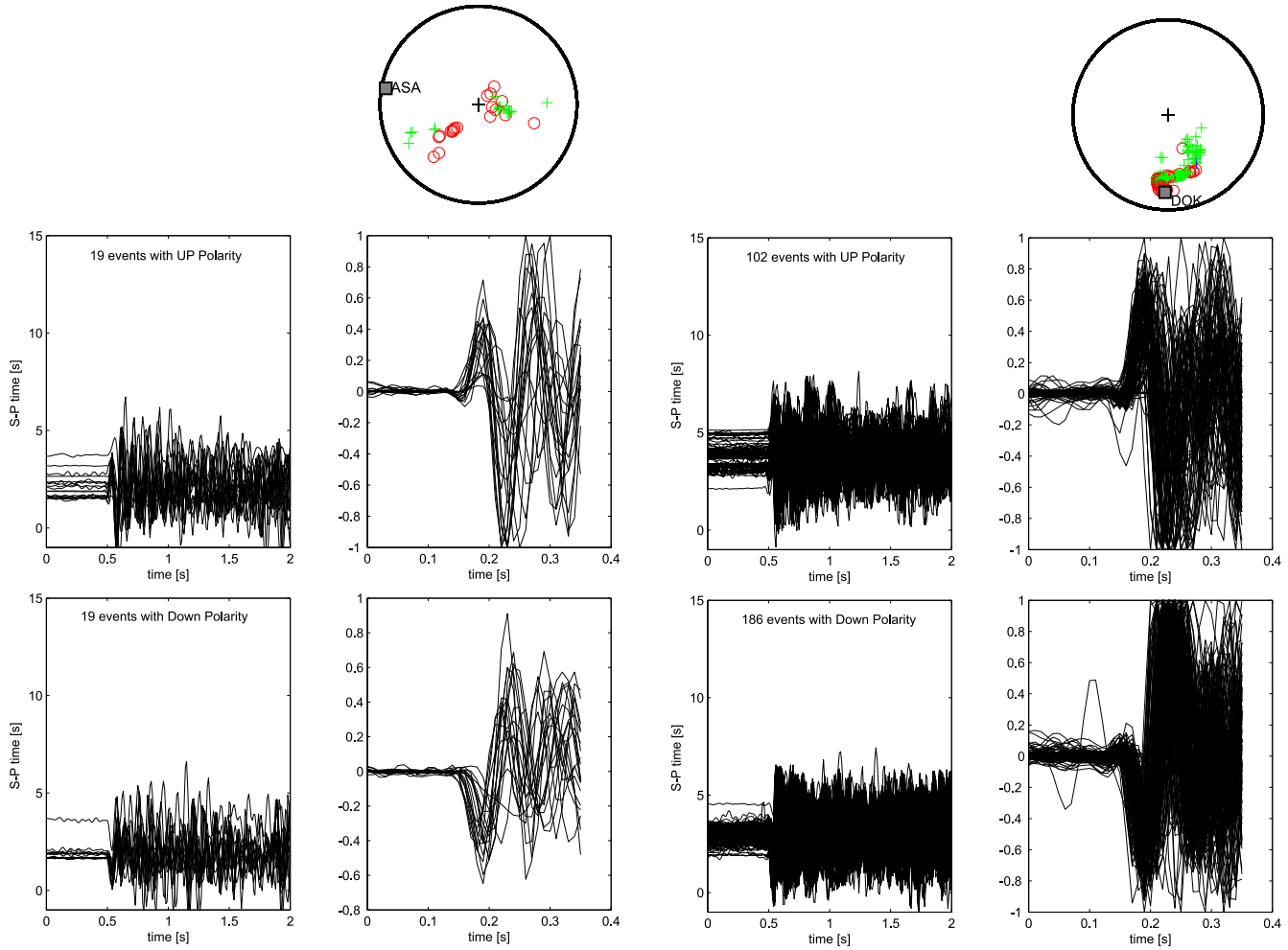

Figure 4. Quality test and first analysis of *P*-wave first-motion polarities for stations ASA and DOK from the SABONET (see Fig. 2 for location). Polarities are separately plotted for positive (upper section) and negative (lower section) for selected seismicity clusters for the year 2000 as part of the post-seismic phase analysed in this study. In addition to the zoomed phase onset plots of the events also the *S–P* time is plotted to give insights into the spatial clustering for the analysed events. Furthermore, in the upper part a summary text with the used number of events with a signal to noise ratio (SNR) > 3 and the focal sphere coverage (crosses-up, circles-down) of the events are given.

of the time-dependent distribution of the events shown in Fig. 6 and their potential focal mechanisms for the subareas a total of nine seismicity clusters were identified and further studied in detail to resolve the particular stress field for different times. Seismic event locations for the different spatial clusters and separated by time are provided in Fig. S1.

4 RESULTS AND DISCUSSION

In the following the results of the stress field orientation obtained by the MOTSI method are described individually for the nine seismicity clusters (summarized in Table 1) from west to east and with time (Figs 7 and 8). All stress inversion results are plotted in lower hemisphere projection with the best solution for the stress orientation of the maximum (σ_1) and minimum (σ_3) principal stress being indicated. For all results the marginal confidence limits in location of the stress axis σ_1 and σ_3 are colour coded from blue (minimum) to red (maximum; Abers & Gephart 2001). Note that the colour-coding is slightly changing for each stress result depending on how well constrained each stress direction is. The distribution of *P*- and *T*-axes from the focal mechanisms calculated by MOTSI (Figs S2 and S3) and the 3-D rotation angles (calculated following Kagan 1991) between cardinal *P*/*T* axis orientation of each focal mechanism and the corresponding stress tensor orientation (Figs S4 and S5) show a large enough spread to ensure that the stress tensor orientation is well constrained. Note that high rotation angle values might be obtained for regions where strike-slip and normal faulting events are occurring within a small area (transtensional stress regime).

4.1 Izmit-Sapanca fault (cluster A)

Cluster A covers the Izmit-Sapanca fault (Fig. 1) and includes the Izmit mainshock epicentre. Since the seismic activity here is very low for the post-seismic period, the results for the stress field orientation are stable only for the pre- and inter Izmit-Düzce phase (Fig. 7). The stress inversion results indicate a clear strike slip (SS) regime for the pre-seismic phase with σ_1 trending ∼N125°E in good accordance with the regional stress field (Kiratzi 2002; Bohnhoff *et al.* 2006; Örgülü 2011). Interestingly, there is a clear change in the local stress field observed along the Izmit-Sapanca fault during the inter Izmit-Düzce phase. The Izmit mainshock introduced a significant anti-clockwise rotation of the minimum principal

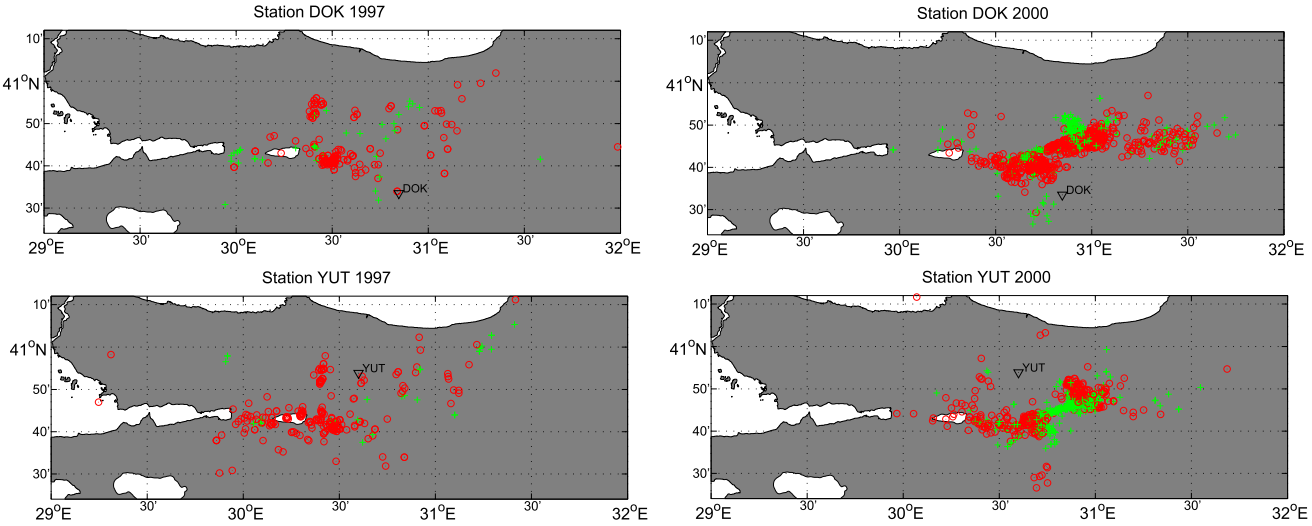

Figure 5. Spatial distribution of first-motion polarities for stations DOK and YUT for the years 1997 (left-hand panel, part of the pre-seismic phase) and 2000 (right-hand panel, part of the post-seismic phase), respectively. First motions are indicated by green crosses and red circles for the positive and negative polarities, respectively. The distribution shows a clear spatial clustering of polarities indicating similar faulting mechanisms in specific areas as a pre-requisite for defining the nine spatial seismicity clusters analysed in this study.

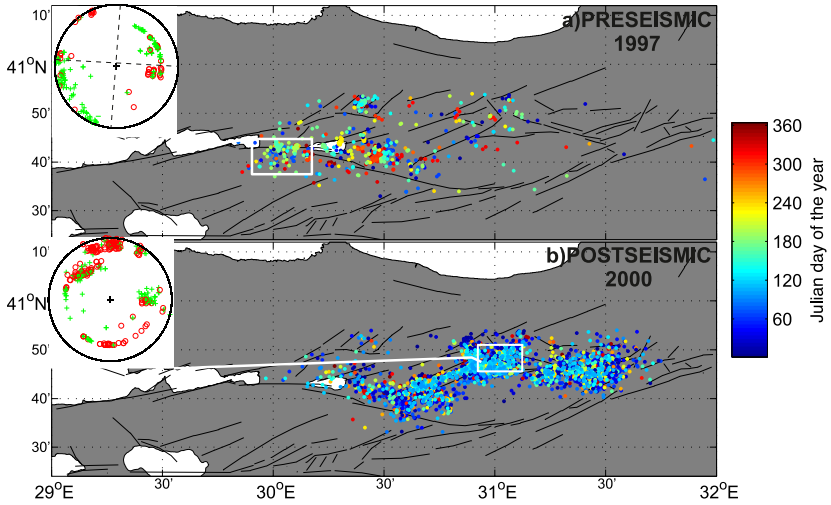

Figure 6. Spatial distribution of the combined seismicity catalogue for the pre-seismic (a) and post-seismic (b) phase of the Izmit and Düzce earthquakes. The temporal evolution for each year is indicated by the colour bar for the specific days of the year (doy). White boxes mark example clusters for which the focal sphere coverage is plotted in the insets in the upper left. Red circles indicate negative, green crosses positive polarities. For the pre-seismic phase as example a predominant strike-slip mechanism for the Izmit-Sapanca area can be assumed (dashed line).

Table 1. Seismicity clusters along the Izmit and Düzce ruptures derived from spatial clustering of local seismicity (A–I) and respective stress field regimes for the pre-seismic, inter Izmit-Düzce and post-seismic phase as obtained from inverting first-motion polarities using the MOTSI method. Strike slip (SS) and normal faulting (NF) refer to strike-slip and normal faulting stress regimes while '?' indicates less-well resolved regimes.

Cluster	Area	Stress inversion results		
ID		Pre-seismic	Inter Izmit-Düzce	Post-seismic
A	Izmit-Sapanca fault	SS	SS/NF	–
B	Sakarya fault	NF	NF	NF/SS?
C	Adapazari-Akyazi basin	NF	NF	NF/SS
D	Karadere fault	NF/SS?	NF	NF
E	Karadere fault south		NF	NF
F	Karadere fault north		SS	SS
G	Düzce fault		SS	SS
H	Düzce basin		SS	SS
I	Elmalik fault		–	SS

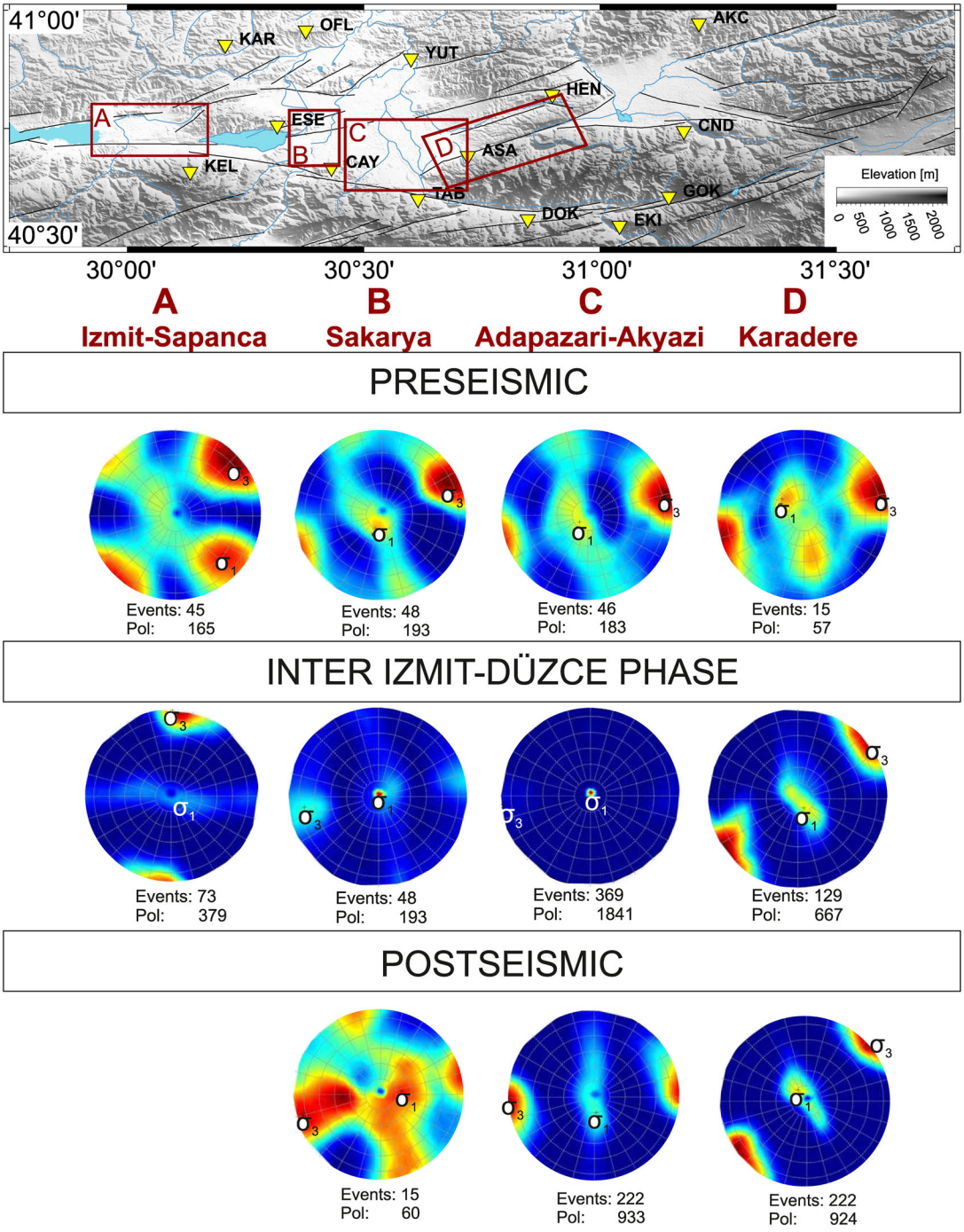

Figure 7. Stress field orientations along the Izmit/Düzce rupture for seismicity clusters A–D marked with red boxes in the upper map view of the Izmit-Düzce rupture. Fault lines (black) are modified after Saroglu (1985), topography: SRTM30 grid. Stress inversion results are calculated using the MOTSI procedure based on first-motion polarities. All results are plotted in lower hemisphere projection. The best solution for the maximum and minimum principal stress ($\sigma_{1;3}$) is indicated. For all results the marginal confidence limits for σ_1 and σ_3 are calculated and plotted colour coded from blue (minimum) to red (maximum).

stress axis (σ_3) of 40 ± 20° and a north-south extensional normal faulting/transtensional component (σ_1 vertical, σ_3 subhorizontal trending NS). This is the first time a well-constrained stress field orientation could be determined for the time just prior to a major earthquake along the entire NAFZ allowing to compare the pre-seismic setting with the setting immediately after a major rupture. Pinar *et al.* (2010) analyzed the stress field orientation in distinct Izmit aftershock clusters based on the inversion of first-motion polarity data using the method of Horiuchi *et al.* (1995). They observed a similar counter-clockwise rotation of 20–25° for the minimum stress direction. Although the coseismic displacement along this part of the Izmit rupture is smaller than on the adjacent Sakarya segment (~3 m), the rotation may also result from stress rotations caused by large Coulomb failure stress changes due to large displacement on strike-slip faults (King *et al.* 1994). This concept of stress rotation has been further investigated and enlarged to

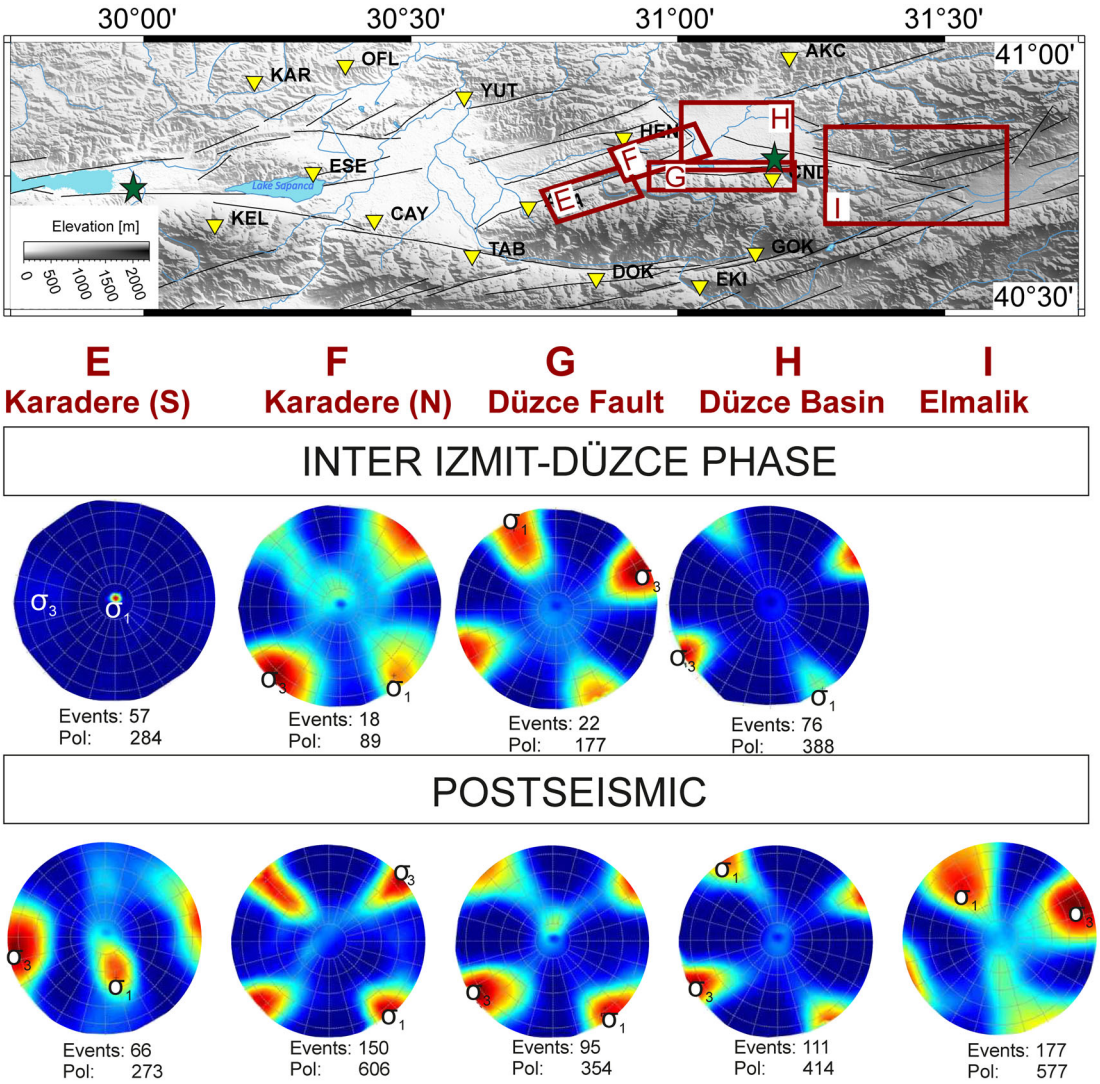

Figure 8. Stress Evolution along the Izmit/Düzce rupture for seismicity clusters E–I marked by the red boxes in the upper map view of the Izmit-Düzce rupture. For detailed figure description please see Fig 7.

subduction zone earthquakes as shown by, for example Hardebeck & Hauksson (2001), Wesson & Boyd (2007), Hasegawa *et al.* (2011) and Yang *et al.* (2013).

In addition, there might also be an influence from the extensional pull-apart basins further to the east (Akyazi) and to the west (Cinarcik) where several east–west-extensional normal faulting aftershocks were observed. The results for the post-seismic phase are poorly resolved due to the decay in seismicity in this area and do not allow for an in-depth analysis of the stress field orientation during the post-seismic phase.

4.2 Sakarya fault (cluster B)

Cluster B is located east of the Sapanca Lake following the main fault trace of the NAFZ along the strike-slip Sakarya fault and crossing the Adapazari-Akyazi Basin (Fig. 1). This area is considered separately from the following Cluster C, because of the presumably different setting (vertical strike-slip fault for the Sakarya fault and pull-apart for the Adapazari-Akyazi Basin) based on a clear difference distribution of first-motion polarities. The Sakarya fault appears to be dominated by the extensional Adapazari-Akyazi Basin already prior to the Izmit earthquake. Stress inversion results indicate a pre-dominant NE–SW extensional normal faulting regime for the whole time period with a slight transtensional component during the pre- and post-seismic phase. During the inter Izmit-Düzce phase a roughly east-west extensional normal faulting regime is observed. In addition, a small clockwise rotation of σ_3 of $\sim 10^\circ$ could have been introduced by the Izmit main shock, although this rotation is not significant within the estimated errors for the stress orientations. The results confirm the observation from Pinar *et al.* (2010) proposing smaller stress rotations on the Sakarya fault compared to the Akyazi Plain (see also Ickrath *et al.* 2014). A possible explanation for this observation is the higher coseismic slip together with lower post-seismic slip along this cluster compared to the Akyazi plain (Langridge *et al.* 2002). In summary, the stress field along the Sakarya fault shows very similar orientation as for the nearby Akyazi pull-apart basin to a large extent.

4.3 Adapazari-Akyazi basin (cluster C)

Cluster C extends throughout the Adapazari-Akyazi basin and lies east of the triple junction formed by the east–west trending Sakarya

fault, the NE-trending Karadere fault and the ESE-striking Mudurnu fault (Fig. 1). The Mudurnu fault was activated in 1967 by a $M > 7$ event and did not show any coseismic slip or aftershock activity related to the Izmit and Düzce events (e.g. Reilinger *et al.* 2000; Bulut *et al.* 2007). It is therefore considered that the Mudurnu fault is still at the early stage of its seismic cycle and no major stress built-up has occurred yet (Langridge *et al.* 2002). The Adapazari-Akyazi basin is hosting the Akyazi gap which is characterized by very low aftershock activity and no recognized co-seismic slip at the surface (Fig. 1). This cluster is of special interest for this study, since the focal mechanism database was too sparse for the time prior to the Izmit event to determine a local stress tensor, while a stable stress field could be determined for the complete time period here from first-motion polarities. Here, the temporal evolution of the stress field in this cluster is investigated in detail indicating a slight change from a NF regime with minor SS components during the pre-seismic phase to pure east–west extensional NF during the inter Izmit-Düzce phase. In the post-seismic phase a backrotation towards the pre-seismic NF/SS regime is observed. It thus allows to investigate in more detail how the pull-apart structure was affected by the Izmit rupture. The detailed analysis shows that the pull-apart structure is generally dominated by a NF stress field already during the pre-seismic time and with only minor temporal variations after the main shock. The minimum principal stress axis σ_3 is nearly stable at a trend of $\sim$85° throughout the whole time period considered here. These refined observations do not fully agree with the proposed idea of our previous study (Ickrath *et al.* 2014), that also in the Adapazari-Akyazi the stress field evolved from the pre-seismic strike slip regime to a dominantly NF-regime and then rapidly recovered to the pre-seismic strike slip regime following the stress-recovery model. But these observations are consistent with Hearn *et al.* (2009) who investigated post-seismic deformation along the Izmit rupture by modelling slip distributions. The authors found evidence for a residual normal faulting component of NS-extension at the Akyazi Plain on a long-term scale. Concluding that coseismic relaxation takes place in effective viscosity of lower crust and upper mantle, the observed extension is caused by the transfer of background tectonic stress to the upper crust. This is also investigated by Stierle *et al.* (2014a,b) who studied the resolution capability of combined SABONET/GTF network for determining non-double-couple components in the seismic moment tensor. The authors obtained significant positive non-double-couple components in the moment tensors of 17 Izmit aftershocks along the Akyazi cluster and suggested local extension and tensile fracturing below the Akyazi Plain possible related to fluid motion in the upper crust. The study from Greber (1994) who investigated circulations of hot palaeo-waters supports this suggestion by finding hot mineral springs restricted to extensional structures within the seismically active NAFZ. In summary, these observations point towards significant structural changes and fault segmentation along the trace of the NAFZ affecting displacement and slip transfer for the entire seismic cycle.

4.4 Karadere fault (cluster D)

Cluster D covers the easternmost portion ruptured during the 1999 August 17 Izmit earthquake and it is dominated by an abrupt change in strike of the NAFZ from east-west to NNE (N65°E; Dikibaş & Akyüz 2011) along the Karadere fault. Iio *et al.* (2002) found evidence for post-seismic slip or creeping along this fault segment which is also confirmed by GPS data analysed by Reilinger *et al.* (2000) and Bürgmann *et al.* (2002) indicating that the highest coseismic slip at depth occurred below the Karadere event cluster. The stress inversion results are nearly consistent throughout the whole time period indicating a NF regime with a small strike slip component in agreement with Ickrath *et al.* (2014). However, it should be noted that the number of events used for the pre-seismic period is quite low and therefore the resolution on the stress field during that time is limited. Using first motion polarity for stress inversion and an extended data base allows subdividing the Karadere fault into two subclusters [southwest (E) and northeast (F), see Fig. 8] which show significantly different stress inversion results. These are discussed in more detail in the following section.

The following five clusters are dominated by aftershocks of the Izmit and Düzce earthquakes and do not host enough seismic events during the pre-seismic phase to investigate the local stress field orientation. Therefore only results for the inter Izmit-Düzce and post-seismic phase are shown and discussed (Fig. 8).

4.5 Karadere fault south (cluster E) and Karadere fault north (cluster F)

While the southern Karadere fault (cluster E) reflects a clear normal faulting regime for the inter Izmit-Düzce and post-seismic phase, the northern Karadere fault (cluster F) reflects a clear strike slip regime. In addition, a significant change in orientation of the minimum principal stress axis σ_3 from nearly east–west for the southern part to N45°E at the northern part is observed. This pattern was also observed by Seeber *et al.* (2000) who found highly diverse focal mechanisms reflecting normal faulting as well as strike slip mechanisms. Moment tensor solutions from Stierle *et al.* (2014b) also indicate a normal faulting regime at the southern part of the Karadere fault stressing the influence of the nearby east–west extensional Akyazi pull-apart basin. Koulakov *et al.* (2010) investigated the distribution of *Vp*, *Vs* and attenuation in the crust beneath the fault based on local earthquake tomography. They found evidence for the opening of a pull-apart zone near the western edge of the Almacik Block (Fig. 1) indicated by weak and moderate seismicity and low seismic velocities. That could explain the existence of the normal faulting characteristic along the southern Karadere fault. In contrast, the northern part of the Karadere fault reflects a clear strike slip regime in accordance with the local morphology and no dominant influence from the Düzce basin located further to the east is seen.

4.6 Düzce fault (cluster G)

Cluster G includes the Düzce fault which splays out from the WSW–ENE trending Karadere fault and represents a major fault asperity. This part of the fault was seismically activated by the Izmit rupture resulting in considerable aftershock activity. However, the rupture did not proceed further to the east until 87 d later when the Düzce earthquake nucleated here (Lettis *et al.* 2002; Peng & Ben-Zion 2006; Görgün *et al.* 2010; Li *et al.* 2014). The Düzce fault represents an east–west-trending strike-slip fault that is also consistent with the resulting stress inversion results with a subhorizontal maximum principal stress axis σ_1 striking N135°E in good accordance with the regional stress field. No temporal variation is seen. The change in fault geometry from the Karadere fault to the Düzce fault was also investigated by Tibi *et al.* (2001) who analysed focal mechanisms of two subevents as part of the Izmit earthquake at the triple junction of the northern Karadere fault and Düzce fault. Both events indicated

an east–west-trending strike slip mechanism fault similar to the Izmit mainshock but have shallower dips (around 60°) than the Izmit main shock (82°) but similar to the focal mechanism of the Düzce main shock (62°).

4.7 Düzce basin (cluster H)

Cluster H is dominated by the Düzce pull-apart basin with irregular eastern and western margins that are bounded by NE–SW mainly right-lateral striking faults and NW–SE striking normal faults (Ardel 1965). Epicentral distribution for the inter Izmit-Düzce and pre-seismic phase (Fig. 2) shows that only the southern part of the Düzce Basin hosts pronounced seismicity. This was also discussed by Pucci *et al.* (2006) who pointed out that the northern part of the basin is no longer active. The basin is dominated by one single river stream that flows northward from the Efteni Lake and crosses orthogonally the northern Karadere fault. It was concluded that only the westernmost part of the Düzce basin is the current 'fault related floodplain' (Pucci *et al.* 2006). This is also supported by the local stress field orientation obtained here (see also Görgün *et al.* 2010). A predominant SS regime with only a small normal faulting component for the inter Izmit-Düzce phase is observed. These observations confirm that the seismicity in the southern branch of the Düzce basin is dominated by the Düzce fault and that the northern branch is presumably inactive.

4.8 Elmalik fault (cluster I)

Cluster I represents the easternmost extension of the Düzce fault and the rupture zone of the Düzce earthquake. This cluster has not been studied in detail previously since no surface slip was observed and no aftershocks were analysed. The WNW/ESE-trending Elmalik fault connects the Düzce fault with the single trace of the NAFZ further to the east (Fig. 1; Akyüz *et al.* 2002; Langridge *et al.* 2002; Pucci *et al.* 2006) where the 1944 M 7.3 earthquake occurred. The fault probably merges with the single principal fault trace of the NAFZ near the city of Bolu. The stress inversion result indicates a strike slip regime with a normal faulting component with a NNW–SSE (N170°E) striking σ_1 which would confirm the geological observations and the trend that the fault is probably merging to the single principal fault trace of the NAFZ near the city of Bolu.

5 CONCLUSIONS

We investigated the stress field evolution in conjunction with the Izmit and Düzce 1999 $M > 7$ main shocks along the NAFZ in NW Turkey. A significantly enlarged event database was used to investigate the stress field orientation in space and time with unprecedented detail inverting first-motion polarities from local seismicity before, between and after the Izmit and Düzce earthquakes. For the determination of the stress field orientation the MOTSI procedure was used, allowing covering areas and time periods for which no sufficient single-event focal mechanisms were available. The results were compared to previous stress inversion studies based on focal mechanisms from the same region and time period. Thereby, the robustness of results obtained by MOTSI could be tested. As Balfour *et al.* (2005) figured out by comparison of confidence intervals of focal mechanisms based and first-motion based inversions, the confidence intervals for the results obtained with MOTSI are often larger but still show significant stress field rotations. Although Robinson & McGinty (2000) suggested that ∼500 polarity observations are required for a robust result, this study shows that also a smaller number of polarities is sufficient to get stable and reasonably resolved stress inversion results. However, the minimum number of polarities needed is probably also depending on the level of stress heterogeneity and spatial segmentation of the study area. It is therefore suggested to carefully analyse the spatial distribution of polarities before their inversion for the stress tensor. For the analysis of large data sets with events of $M \leq 3$ the first motion based stress inversion is preferred, since for small events only few focal mechanisms may be available. Using first motion polarity a larger number of small events can be taken into account and due to the error assessment the results give a better indication of the real uncertainties.

In this study nine distinct seismicity clusters were investigated for the first time separately for the pre-, inter Izmit-Düzce and post-seismic phase covering the combined Izmit-Düzce rupture and surrounding areas and time intervals for which no sufficient single-event focal mechanisms were available. Fig. 9 summarizes the results obtained in this study. The Izmit-Sapanca fault (cluster A) displays a stable strike-slip region for the pre-seismic phase in accordance with the regional, long-term stress regime. After the Izmit main shock this turns into a normal faulting regime influenced by the pull-apart Adapazari-Akyazi basin further to the east. The Sakarya fault (cluster B) is generally dominated by the neighbouring Akyazi pull-apart basin. Thereby a small change from substantially normal faulting influence in the pre-seismic phase to completely dominated in the inter Izmit-Düzce phase to a slightly start of a back-rotation to strike slip in the post-seismic phase can be distinguished. Further to the east, the Akyazi plain (cluster C) representing a pull-apart structure that hosted a 3.5 m coseismic slip deficit is dominated by the EW-extensional normal faulting regime combined with a strike-slip component for the pre-seismic phase. Whereas the southern Karadere fault (cluster E) showing a normal faulting regime is still dominated by the extensional regime in the Akyazi plain, the northern Karadere fault (cluster F) seems to be connected with the Düzce fault reflecting a strike-slip regime. The influence of the normal faulting regime seems to be concentrated around the Akyazi plain and no influence can be observed further to the east or west onto strike-slip faults (Sakarya, Karadere). Also the Düzce fault (cluster G) reflects a stable strike-slip regime and is not influenced by the Düzce pull-apart basin (cluster H) which has similar characteristics like the Akyazi plain but no temporal change in the stress regime is observable, probably because no major coseismic slip deficit occurred. Finally, the Elmalik fault (cluster I) was characterized for the first time indicating a strike-slip regime.

In summary, the stress field evolution of the studied clusters along the Izmit and Düzce ruptures can be followed from the predominantly pre-seismic strike-slip regime in the west, the inter Izmit-Düzce phase of the dominant east-west extensional regime in the Akyazi plain to the nearly stable post-seismic strike-slip regime along the Düzce and Elmalik faults corresponding to the regional stress field.

ACKNOWLEDGEMENTS

This study was funded by the Helmholtz Association in the frame of the Young Investigators Group 'From Microseismicity to Large Earthquakes'. We gratefully acknowledge provision of seismic waveforms from the GTF (German Task Force for Earthquakes) and SABONET networks and especially thank J. Zschau and C. Milkereit. A special thanks goes to G. Abers for providing the MOTSI stress inversion software. Most of the figures were created

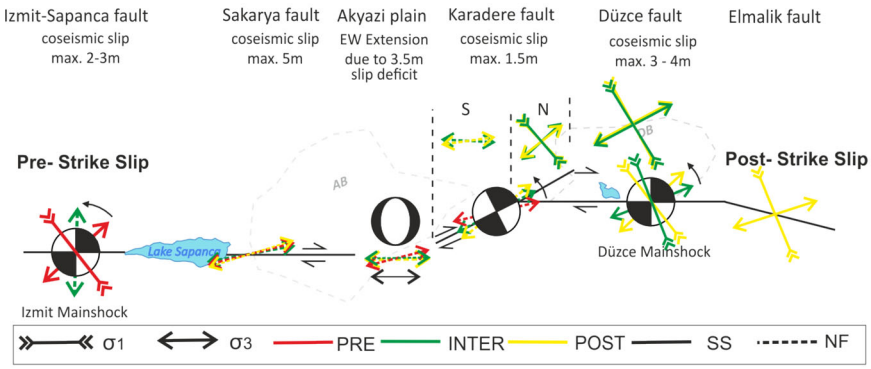

Figure 9. Combined stress inversion results along distinct segments of the Izmit and Düzce rupture based on the inversion from focal mechanism and first motion polarities. Focal mechanisms indicate the predominantly regime in the distinct area. The stress evolution corresponding to the rotation of the minimum principal stress axis (σ_3, arrows pointing outwards) along the fault can be followed by the colour-coded bars, indicating the pre-, inter Izmit-Düzce and post-seismic state of stress in red, green and yellow, respectively. When the σ_1 is horizontal, its orientation is plotted with arrows pointing inwards. Solid lines indicate strike-slip regime while dashed lines refer to normal faulting environment. The regional direction of the maximum principal stress axis (σ_1) is given in the legend for the colour coding of the bars. The amount of coseismic slip for each cluster is given below the clusters names. AB, Adapazari-Akyazi Basin; DB, Düzce Basin.

with the GMT software (Wessel & Smith 1998). We thank the editor E. Hauksson and two anonymous reviewers for constructive comments that helped to improve the manuscript.

REFERENCES

Abers, G.A. & Gephart, J.W., 2001. Direct inversion of earthquake first motions for both the stress tensor and focal mechanisms and application to Southern California, *J. geophys. Res.,* **106**(B11), 26 523–26 540.

Akyüz, H., Hartleb, R., Barka, A., Altunel, E., Sunal, G., Meyer, B. & Armijo, R., 2002. Surface rupture and slip distribution of the 12 November 1999 Düzce earthquake (M 7.1), North Anatolian Fault, Bolu, Turkey, *Bull. seism. Soc. Am.,* **92**(1), 61–66.

Ardel, A., 1965. Anadolu havzalarinin tesekkül ve tekâmülü hakkinda düsünceler, *Istanbul Univ. Cograf. Enst. Derg,* **8**(15), 60–73.

Balfour, N., Savage, M. & Townend, J., 2005. Stress and crustal anisotropy in Marlborough, New Zealand: evidence for low fault strength and structure-controlled anisotropy, *Geophys. J. Int.,* **163**(3), 1073–1086.

Barka, A., 1999. The 17 August 1999 Izmit earthquake, *Science,* **285**(5435), 1858–1859.

Barka, A. *et al.*, 2002. The surface rupture and slip distribution of the 17 August 1999 Izmit earthquake (M7.4), North Anatolian Fault, *Bull. seism. Soc. Am.,* **92**(1), 43–60.

Baumbach, M. *et al.*, 2003. Calibration of an ML scale in northwestern Turkey from 1999 Izmit aftershocks, *Bull. seism. Soc. Am.,* **93**(5), 2289–2295.

Bindi, D., Parolai, S., Gorgun, E., Grosser, H., Milkereit, C., Bohnhoff, M. & Durukal, E., 2007. ML scale in northwestern Turkey from 1999 Izmit Aftershocks: updates, *Bull. seism. Soc. Am.,* **97**(1B), 331–338.

Bohnhoff, M., Baisch, S. & Harjes, H.-P., 2004. Fault mechanisms of induced seismicity at the superdeep German Continental Deep Drilling Program (KTB) borehole and their relation to fault structure and stress field, *J. geophys. Res.,* **109**(B2), doi:10.1029/2003JB002528.

Bohnhoff, M., Grosser, H. & Dresen, G., 2006. Strain partitioning and stress rotation at the North Anatolian fault zone from aftershock focal mechanisms of the 1999 Izmit $M_w = 7.4$ earthquake, *Geophys. J. Int.,* **166**(1), 373–385.

Bohnhoff, M., Bulut, F., Dresen, G., Malin, P.E., Eken, T. & Aktar, M., 2013. An earthquake gap south of Istanbul, *Nat. Commun.,* **4**, 1999, doi:10.1038/ncomms2999.

Bulut, F., Bohnhoff, M., Aktar, M. & Dresen, G., 2007. Characterization of aftershock fault plane orientations of the 1999 Izmit (Turkey) earthquake using high-resolution aftershock locations, *Geophys. Res. Lett.,* **34**(20), L20306, doi:10.1029/2007GL031154.

Bulut, F., Bohnhoff, M., Eken, T., Janssen, C., Kılıç, T. & Dresen, G., 2012. The East Anatolian fault zone: seismotectonic setting and spatiotemporal characteristics of seismicity based on precise earthquake locations, *J. geophys. Res.,* **117,** B07304, doi:10.1029/2011JB008966.

Bürgmann, R., Ergintav, S., Segall, P., Hearn, E., McClusky, S., Reilinger, R., Woith, H. & Zschau, J., 2002. Time-dependent distributed afterslip on and deep below the Izmit earthquake rupture, *Bull. seism. Soc. Am.,* **92**(1), 126–137.

Dikibaş, A. & Akyüz, H.S., 2011. Palaeoseismological investigations on the Karadere segment, North Anatolian fault zone, Turkey, *Turk. J. Earth Sci.,* **20**(4), 395–410.

Gephart, J.W., 1990. Stress and the direction of slip on fault planes, *Tectonics,* **9**(4), 845–858.

Görgün, E., Bohnhoff, M., Bulut, F. & Dresen, G., 2010. Seismotectonic setting of the Karadere-Düzce branch of the North Anatolian Fault Zone between the 1999 Izmit and Düzce ruptures from analysis of Izmit aftershock focal mechanisms, *Tectonophysics,* **482,** 170–181.

Greber, E., 1994. Deep circulation of CO_2-rich paleowaters in a seismically active zone (Kuzuluk/Adapazari, northwestern Turkey), *Geothermics,* **23**(2), 151–174.

Grosser, H. *et al.*, 1998. The Erzincan (Turkey) earthquake (Ms 6.8) of March 13, 1992 and its aftershock sequence, *PAGEOPH,* **152**(3), 465–505.

Hardebeck, J.L. & Hauksson, E., 2000. The San Andreas fault in Southern California: a weak fault in a weak crust, in *Proceedings of the 3rd Conf. on Tectonic Problems of the San Andreas Fault System*, Stanford, California.

Hardebeck, J.L. & Hauksson, E., 2001. Crustal stress field in southern California and its implications for fault mechanics, *J. geophys. Res.,* **106**(B10), 21 859–21 882.

Hardebeck, J.L. & Michael, A.J., 2004. Stress orientations at intermediate angles to the San Andreas fault, California, *J. geophys. Res.,* **109,** B11303, doi:10.1029/2004JB003239.

Hasegawa, A., Yoshida, K. & Okada, T., 2011. Nearly complete stress drop in the 2011 M_w 9.0 off the Pacific coast of Tohoku earthquake, *Earth Planets Space,* **63,** 703–707.

Hearn, E., McClusky, S., Ergintav, S. & Reilinger, R., 2009. Izmit earthquake postseismic deformation and dynamics of the North Anatolian fault zone, *J. geophys. Res.,* **114**(B8), doi:10.1029/2008JB006026.

Horiuchi, S., Rocco, G. & Hasegawa, A., 1995. Discrimination of fault planes from auxiliary planes based on simultaneous determination of stress tensor and a large number of fault plane solutions, *J. geophys. Res.,* **100**(B5), 8327–8338.

Hubert-Ferrari, A., Barka, A., Jacques, E., Nalbant, S.S., Meyer, B., Armijo, R., Tapponnier, P. & King, G.C., 2000. Seismic hazard in the Marmara Sea region following the 17 August 1999 Izmit earthquake, *Nature,* **404**(6775), 269–273.

Ickrath, M., Bohnhoff, M., Bulut, F. & Dresen, G., 2014. Stress rotation and recovery in conjunction with the 1999 Izmit M_w 7.4 earthquake, *Geophys. J. Int.,* **196**(2), 951–956.

Iio, Y., Horiuchi, S., Bariş, Ş., Celik, C., Kyomen, J., Üçer, B., Honkura, Y. & Işikara, A.M., 2002. Aftershock distribution in the eastern part of the aftershock region of the 1999 Izmit, Turkey, earthquake, *Bull. seism. Soc. Am.,* **92**(1), 411–417.

Kagan, Y.Y., 1991. 3-D rotation of double-couple earthquake sources, *Geophys. J. Int.,* **106,** 709–716.

King, G., Stein, R. & Lin, J., 1994. Static stress changes and the triggering of earthquakes, *Bull. seism. Soc. Am.,* **84**(3), 935–953.

Kiratzi, A.A., 2002. Stress tensor inversions along the westernmost North Anatolian fault zone and its continuation into the North Aegean Sea, *Geophys. J. Int.,* **151**(2), 360–376.

Koulakov, I., Bindi, D., Parolai, S., Grosser, H. & Milkereit, C., 2010. Distribution of seismic velocities and attenuation in the crust beneath the North Anatolian fault (Turkey) from local earthquake tomography, *Bull. seism. Soc. Am.,* **100**(1), 207–224.

Langridge, R., Stenner, H., Fumal, T., Christofferson, S., Rockwell, T., Hartleb, R., Bachhuber, J. & Barka, A., 2002. Geometry, slip distribution, and kinematics of surface rupture on the Sakarya fault segment during the 17 August 1999 Izmit, Turkey, earthquake, *Bull. seism. Soc. Am.,* **92**(1), 107–125.

Lee, W. & Lahr, J., 1972. HYPO-71 a computer program for determining hypocenter, magnitude and first motion pattern of local earthquakes, *Open-File Report. US Geol. Surv.,* Menlo Park, CA.

Lettis, W., Bachhuber, J., Witter, R., Brankman, C., Randolph, C., Barka, A., Page, W. & Kaya, A., 2002. Influence of releasing step-overs on surface fault rupture and fault segmentation: examples from the 17 August 1999 Izmit earthquake on the North Anatolian fault, Turkey, *Bull. seism. Soc. Am.,* **92**(1), 19–42.

Li, Z., Zhang, H. & Peng, Z., 2014. Structure-controlled seismic anisotropy along the Karadere Düzce branch of the North Anatolian Fault revealed by shear-wave splitting tomography, *Earth planet. Sci. Lett.,* **391,** 319–326.

Lienert, B.R., Berg, E. & Frazer, L.N., 1986. HYPOCENTER: an earthquake location method using centered, scaled, and adaptively damped least squares, *Bull. seism. Soc. Am.,* **76**(3), 771–783.

Lienert, B.R. & Havskov, J., 1995. A computer program for locating earthquakes both locally and globally, *Seismol. Res. Lett.,* **66**(5), 26–36.

Michael, A.J., 1987. Stress rotation during the Coalinga aftershock sequence, *J. geophys. Res.,* **92,** 7963–7979.

Milkereit, C. *et al.*, 2000. Preliminary aftershock analysis of the $M_w = 7.4$ Izmit and $M_w = 7.1$ Düzce earthquake in western Turkey, in *The 1999 Izmit and Düzce Earthquakes: Preliminary Results,* pp. 179–187, eds Kozaci, Ö. & Barka, A., Istanbul Technical University.

Örgülü, G., 2011. Seismicity and source parameters for small-scale earthquakes along the splays of the North Anatolian Fault (NAF) in the Marmara Sea, *Geophys. J. Int.,* **184**(1), 385–404.

Parolai, S., Bindi, D., Baumbach, M., Grosser, H., Milkereit, C., Karakisa, S. & Zunbul, S., 2004. Comparison of different site response estimation techniques using aftershocks of the 1999 Izmit earthquake, *Bull. seism. Soc. Am.,* **94**(3), 1096–1108.

Peng, Z. & Ben-Zion, Y., 2006. Temporal changes of shallow seismic velocity around the Karadere-Düzce branch of the north Anatolian fault and strong ground motion, *Pure appl. Geophys.,* **163**(2–3), 567–600.

Pinar, A., Ucer, S., Honkura, Y. & Sezgin, N., 2010. Spatial variation of the stress field along the fault rupture zone of the 1999 Izmit earthquake, *Earth Planets Sci.,* **62**(3), 237–256.

Pucci, S., Pantosti, D., Barchi, M., Palyvos, N. & Palyvos, N., 2006. Evolution and complexity of the seismogenic Düzce fault zone (Turkey) depicted by coseismic ruptures, Plio-Quaternary structural pattern and geomorphology, *Geophys. Res. Abstr.,* **8,** 08339.

Reilinger, R.E. *et al.*, 2000. Coseismic and postseismic fault slip for the 17 August 1999, M = 7.5, Izmit, Turkey earthquake, *Science,* **289**(5484), 1519–1524.

Robinson, R. & McGinty, P., 2000. The enigma of the Arthur's Pass, New Zealand, earthquake 2. The aftershock distribution and its relation to regional and induced stress fields, *J. geophys. Res.,* **105**(B7), 16 139–16 150.

Saroglu, F., 1985. Dogu Anadolu nun Neotektonik Dönemde Jeolojik ve Yapsal Evrimi, *PhD thesis*, Istanbul Univ.

Seeber, L., Armbruster, J.G., Ozer, N., Aktar, M., Baris, S., Okaya, D., Ben-Zion, Y. & Field, E., 2000. The 1999 earthquake sequence along the North Anatolia transform at the juncture between the two main ruptures, in *The 1999 Izmit and Düzce Earthquakes: Preliminary Results*, pp. 209–223, eds Barka, A., Kozaci, Ö., Akyüz, H.S. & Altunel, E., Istanbul Technical University.

Şengör, A.M.C., Tüysüz, O., İmren, C., Sakınç, M., Eyidoğan, H., Görür, N., Le Pichon, X. & Rangin, C., 2005. The North Anatolian Fault: a new look, *Ann. Rev. Earth planet. Sci.,* **33,** 37–112.

Stierle, E., Vavryčuk, V., Šílený, J. & Bohnhoff, M., 2014a. Resolution of non-double-couple components in the seismic moment tensor using regional networks—I: a synthetic case study, *Geophys. J. Int.,* **196**(3), 1869–1877.

Stierle, E., Bohnhoff, M. & Vavryčuk, V., 2014b. Resolution of non-double-couple components in the seismic moment tensor using regional networks – II: application to aftershocks of the 1999 M_w 7.4 Izmit earthquake, *Geophys. J. Int.,* **503**, doi:10.1029/2008JB006026.

Tibi, R. *et al.*, 2001. Rupture processes of the 1999 August 17 Izmit and November 12 Düzce (Turkey) earthquakes, *Geophys. J. Int.,* **144**(2), F1–F7.

Toksöz, M., Shakal, A. & Michael, A.J., 1979. Space-time migration of earthquakes along the North Anatolian fault zone and seismic gaps, in *Earthquake Prediction and Seismicity Patterns,* pp. 1258–1270, ed. Wyss, M., Springer.

Townend, J. & Zoback, M.D., 2000. Focal mechanism stress inversions in Southern California and the strength of the San Andreas fault, in *Proceedings of the 3rd Conf. on Tectonic Problems of the San Andreas Fault System*, Stanford, California.

Wessel, P. & Smith, W.H.F., 1998. New, improved version of generic mapping tools released, *EOS, Trans, Am. geophys. Un.,* **79**(47), 579–579.

Wesson, R.L. & Boyd, O.S., 2007. Stress before and after the 2002 Denali fault earthquake, *Geophys. Res. Lett.,* **34,** L07303, doi:10.1029/2007GL029189.

Yang, Y.-R., Johnson, K.M. & Chuang, R.Y., 2013. Inversion for absolute deviatoric crustal stress using focal mechanisms and coseismic stress changes: the 2011 M9 Tohoku-oki, Japan, earthquake, *J. geophys. Res.,* **118,** 5516–5529.

SUPPORTING INFORMATION

Additional Supporting Information may be found in the online version of this paper:

Figure S1. Epicentral distribution of seismicity within the different clusters during the pre-Izmit, inter-Izmit-Düzce and post-Düzce seismic periods. Fig. S1 shows the location of the events inverted within each particular time period and for each cluster A–I separately. With the exception of the Izmit-Sapanca area (Cluster A), the amount of seismicity is significantly larger during the inter- and post-seismic periods (where the aftershock activity is distributed throughout most of the study area) than in the pre-seismic period. It is worth to note that the pre-seismic period of the seismicity within Cluster D (Karadere Fault) is mostly occurring at the southwest (near the Adapazari-Akyazi basin), while during the interseismic and post-seismic periods, seismicity is distributed evenly along the entire Karadere Fault. Note that stress field orientation for segments E–I in the pre-seismic period has not been estimated due to reduced number of events.

Figure S2. Distribution of *P*- and *T*-axes within the individual Clusters A–D. Fig. S2 shows the distribution of the *P*- and *T*-axes on the stereo net from the focal mechanism solutions provided

as an output of MOTSI for each of the stress tensor inversions shown in Fig. 7. Red dots represent pressure axes and blue dots represent tensional axes. Visually, the distributions are overall in good agreement with the provided orientation of the stress field in each particular spatial and/or temporal subdivision. These plots show that the pre-seismic stress field orientation for the Karadere Fault has limited resolution due to the low number of events.

Figure S3. Distribution of *P*- and *T*-axes within the individual Clusters E–I. Fig. S3 shows the corresponding *P*- and *T*-axes for the stress tensor inversions shown in Fig. 8 of the main manuscript. Red dots represent pressure axes and blue dots represent tensional axes. Visually, the distributions are overall in good agreement with the provided orientation of the stress field in each particular spatial and/or temporal subdivision.

Figure S4. Histograms of angles between stress field and focal mechanisms (segments A–D). This figure shows the 3-D rotation angle (after Kagan 1991) between the estimated stress field orientation and each corresponding focal mechanism provided as output from MOTSI in the stress inversions shown in Fig. 7 of the main manuscript. The variety of orientations from the focal mechanisms necessary to appropriately constrain the stress field orientation is then confirmed by the median or average value for this angle in each inversion. High values of this angle might be occurring due to the combined occurrence of normal faulting and strike-slip events (transtensional stress regime) at certain areas.

Figure S5. Histograms of angles between stress field and focal mechanisms (segments E–I). This figure shows the 3-D rotation angle (after Kagan 1991) between the estimated stress field orientation and each corresponding focal mechanisms provided as output from MOTSI in the stress inversions shown in Fig. 8. (http://gji.oxfordjournals.org/lookup/suppl/doi:10.1093/gji/ggv273/-/DC1).